Construction and Building Materials 419 (2024) 135523

Contents lists available at ScienceDirect

Construction and Building Materials

journal homepage: www.elsevier.com/locate/conbuildmat

On the use of machine learning and data-transformation methods to predict hydration kinetics and strength of alkali-activated mine tailings-based binders

Sahil Surehali [a], Taihao Han [b], Jie Huang [c], Aditya Kumar [d], Narayanan Neithalath [e,*]

[a] School of Sustainable Engineering and Built Environment, Arizona State University, Tempe, AZ 85287, USA
[b] Department of Materials Science and Engineering, Missouri University of Science and Technology, Rolla, MO 65409, USA
[c] Department of Electrical and Computer Engineering, Missouri University of Science and Technology, Rolla, MO 65409, USA
[d] ADepartment of Materials Science and Engineering, Missouri University of Science and Technology, Rolla, MO 65409, USA
[e] School of Sustainable Engineering and Built Environment, Arizona State University, Tempe, AZ 85287, USA

ARTICLE INFO

Keywords:
Mine tailings
Compressive strength
Hydration kinetics
Machine learning
Sustainability

ABSTRACT

The escalating production of mine tailings (MT), a byproduct of the mining industry, constitutes significant environmental and health hazards, thereby requiring a cost-effective and sustainable solution for its disposal or reuse. This study proposes the use of MT as the primary ingredient ($\geq$70%$_{mass}$) in binders for construction applications, thereby ensuring their efficient upcycling as well as drastic reduction of environmental impacts associated with the use of ordinary Portland cement (OPC). The early-age hydration kinetics and compressive strength of MT-based binders are evaluated with an emphasis on elucidating the influence of alkali activation parameters and the amount of slag or cement that are used as minor constituents. This study reveals correlations between cumulative heat release and compressive strengths at different ages; these correlations can be leveraged to estimate the compressive strength based on hydration kinetics. Furthermore, this study presents a random forest (RF) model—in conjunction with fast Fourier and direct cosine transformation techniques to overcome the limitations associated with limited volume and diversity of the database—to enable high-fidelity predictions of time-dependent hydration kinetics and compressive strength of MT-based binders in relation to mixture design. Overall, this study demonstrates a sustainable approach to upcycle mine tailings as the primary component in low-carbon construction binders; and presents both analytical and machine learning-based approaches for accurate *a priori* predictions of hydration kinetics and compressive strength of these binders.

1. Introduction

Mine tailings (MT) are the waste residues generated after valuable components or metals are extracted from the minerals and ores through mining operations [1]. The mineralogy of MT strongly depends on the type of ore, the mineral processing technology, and the degree of weathering during storage in tailings ponds [2]. The high ratio (~100:1) of tailings to valuable metal/components results in the mining industry producing enormous volumes of MT, making their sustainable disposal a critical environmental concern [3], [4]. The lack of systematic waste disposal strategies has led to most MT being disposed of in tailings ponds or mine waste landfills [5–8]. The immense size and hazardous composition of materials in tailings dams pose immense risk to both aquatic and human life for potentially hundreds of kilometers downstream [9], [10]. Failure of these dams has led to the contamination of floodplains by metal and metalloid elements, which are highly toxic to humans and the environment [11], [12]. Furthermore, the accumulation of tailings could also lead to the release of heavy metals, radioactive elements, and other toxic components, thereby contaminating soils, biota, water, and air [13–16]. To address these environmental concerns, sustainable disposal methods and systematic waste management (e.g., reuse and upcycling) strategies are needed to mitigate the risks associated with MT and safeguard ecosystems and communities from their detrimental effects.

Most MT are composed of oxides of silicon, aluminum, and calcium—oxides that are also present in ordinary Portland cement (OPC) and conventional supplementary cementitious materials (SCMs: e.g., fly ash, slag, and calcined clay) [1], [17], [18]. In light of this congruence in

* Corresponding author.
E-mail address: Narayanan.Neithalath@asu.edu (N. Neithalath).

https://doi.org/10.1016/j.conbuildmat.2024.135523
Received 1 November 2023; Received in revised form 19 January 2024; Accepted 18 February 2024

chemical composition, MT have been considered to be a concrete ingredient [3], [19], [20], [21], [22], potentially capable of imparting twin benefits: reduction of carbon footprint of OPC and beneficial disposal/immobilization of a hazardous waste material. However, the relatively low reactivity and highly heterogeneous composition of MT limit their use as SCM. Even when MT is used as a sole precursor to alkali-activated binders, such binders demonstrate slow setting and low strength [23], [24]. The use of MT in combination with more reactive Ca-containing additives such as slag and OPC has been shown to alleviate these issues [25–28] through the formation of additional hydration products. Considering the high demand for traditional precursor materials for alkali activation (slag, fly ash, etc. ([29–31]) for conventional concrete applications, alongside their increasing scarcity, this study examines the use of large volumes of MT ($\geq$70%$_{mass}$ of the source materials) in combination with small amounts of OPC or slag as "reaction enhancers" in the production of alkali-activated binders. The aim is to produce binders with performance comparable to traditional OPC concretes or *slag-only* alkali-activated concretes for several application scenarios such as grouts, repair materials, and coatings. Furthermore, the stable reaction products of these systems, such as alkali (or alkaline earth) aluminosilicates, are more likely to permanently immobilize harmful ingredients and prevent them from leaching out into the environment [32–34] – a fact also confirmed through our experiments on the MT-based binders reported here. To develop sustainable MT-based binders, it is important to study and explain the effects of varying Na_2O-to-total powder ratios (n), SiO_2-to-Na_2O ratios (M_s), and slag or OPC contents on early-age hydration kinetics and compressive strength development. Furthermore, it is essential to carefully optimize the material design (e.g., additive and activator type and composition, activator parameters and content, etc.) since they exert significant influence on the fresh and hardened properties of the resultant mixture [35–38]. Such an optimization exercise requires a large amount of experimental data, primarily due to the considerable spread of chemical composition of precursors and activator characteristics which essentially dictate the development of all key properties. It is because of this aforesaid spread—and the degrees of freedom that arise from it—that several past attempts to develop direct correlations between chemical compositions of the precursors and compressive strength of alkali-activated binders [39–42] have met with limited success.

In this study, we employ machine learning (ML) methods to predict the performance of MT-based alkali-activated binders. ML techniques have been extensively utilized for predicting properties in traditional concrete, but their applications in developing prediction models for alkali-activated binders are limited [43–45]. Some studies have employed ML models to predict the compressive strength of alkali-activated concrete based on various inputs [44], [46]; but very few have focused on MT-based alkali-activated binders [47–49]. A large number of ML studies on traditional and special-purpose binders rely on predicting the mechanical properties from easy-to-obtain attributes of the mixture (e.g., cement and water contents, source material compositions, etc.). These purely data-driven predictions obviate the need for understanding the underlying mechanisms such as the influence of hydration kinetics on the properties. While a large enough database allows ML algorithms to more efficiently learn inputs-output (i.e., cause-effect) correlations and reasonably predict the performance without uncovering the underlying mechanisms, this approach is fraught with danger when the size of the database is small, as is the case with unique binder systems such as the one under consideration here. It is, thus, important to reduce the degrees of freedom within the database through curated data transformation techniques. Herein, we use fast Fourier transform (FFT) and discrete cosine transform (DCT) methods, alongside a Random Forest (RF) model, to predict both the heat flow rate and the compressive strength of MT-based binders from a limited database.

2. Experimental program

2.1. Materials

MT from a copper mine was used as the primary source material ($\geq$ 70% $_{mass}$), with OPC or slag comprising the remaining ($\leq$30%$_{mass}$). The tailings, which were obtained in a slurry form from Freeport McMoRan Inc. (FMI), were dewatered, oven dried at 80 °C for 24 h, and crushed to a fine powder before using it in the paste and mortar mixtures. Ground granulated blast furnace slag (hereinafter referred to as slag) conforming to ASTM C 989 and Type I/II OPC conforming to ASTM C 150 were used to replace 10%, 20%, and 30% by mass of MT in the binder system. MT, slag, and OPC have median particle sizes (d_{50}) of 38.63 μm, 12.33 μm, and 15.23 μm, respectively, as shown in Fig. 1. The chemical compositions of the binder constituents obtained using X-ray fluorescence (XRF) are summarized in Table 1. MT has a combined ($SiO_2 + Al_2O_3 + Fe_2O_3$) $>$ 85%, meeting the chemical requirements of fly ash as per ASTM C 618. The specific gravities of MT, slag, and OPC were determined to be 2.76, 2.92, and 3.20, respectively, using a gas pycnometer. Sodium silicate solution (waterglass), with a SiO_2–to-Na_2O mass ratio (referred to as M_s) of 1.59 was used as the activation agent. NaOH solution was added to the activator to reduce its M_s values to desired levels. M_s values of 1.0 and 1.5 were chosen in this study as they have been shown to enable efficient activation in our previous works on alkali-activated binders [50], [51].

2.2. Mixture proportions

Slag (S) and cement (C) were used to replace 10%, 20%, and 30% by mass of MT to develop MT-S and MT-C binders respectively. The activation solution comprised sodium silicate, sodium hydroxide (NaOH), and water. The activation solution was proportioned to obtain SiO_2-to-Na_2O ratios (M_s) of 1.0 and 1.5, and Na_2O-to-total powder ratio (n) varying from 0.025 to 0.1 in increments of 0.025. All MT-S binders were prepared using a liquid-to-binder (l/b) ratio of 0.35, and the MT-C binders comprising 10%, 20%, and 30% cement content mass were prepared using l/b ratios of 0.40, 0.45, and 0.55, respectively. The l/b ratios were varied in this case to ensure that the mixtures remained workable (for details, readers are referred to [52]) for at least 15 min as rapid coagulation is reported to result in quick setting of alkali activated mixtures [53]. Companion rheological experiments indicated that the yield stress and plastic viscosity of the MT-S blends varied between 2 and 5 Pa and 1–6 Pa.s respectively, while those of the MT-C blends varied between 10 and 50 Pa and 0.05–0.3 Pa.s respectively.

Initially, the NaOH solution was prepared and allowed to cool down to ambient temperature. Liquid sodium silicate with an M_s value of 1.59 was added to arrive at the desired M_s values for the mixtures, which

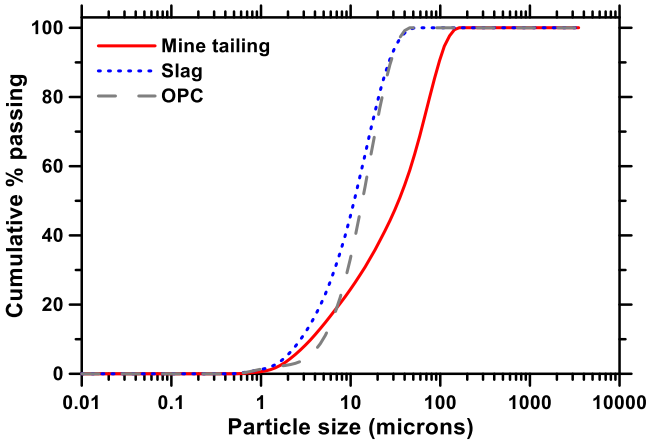

Fig. 1. Particle size distribution curves for MT, slag, and cement.

Table 1
Chemical composition of the binder ingredients.

Binder ingredients	Chemical composition								
Mine tailings (MT)	SiO_2 (%)	Al_2O_3 (%)	SO_3 (%)	Fe_2O_3 (%)	Sn (%)	Mn (%)	Ti (%)	Sb (%)	P (%)
	64.2	19.95	1.94	8.26	1.35	0.81	0.48	2.49	0.15
	SiO_2 (%)	Al_2O_3 (%)	SO_3 (%)	Fe_2O_3 (%)	MgO (%)	Na_2O (%)	K_2O (%)	CaO (%)	LOI* (%)
GGBFS (S)	39.4	8.49	2.83	0.37	12.05	0.27	0.80	35.53	1.31
OPC (C)	21.3	3.78	2.88	3.75	1.77	0.25	0.17	63.83	1.34

* Loss on Ignition

were 1.0 and 1.5, as mentioned earlier. The activator solution was then mixed with the binder ingredients. The sequential procedure to determine the quantities of the activator solution is elaborated in detail in our previous work [36], [37]. The mortar mixtures prepared for compressive strength tests comprised 50% river sand by total mortar volume.

2.3. Test methods

Isothermal calorimetry experiments were carried out following ASTM C 1679. The pastes were mixed externally and loaded into the isothermal calorimeter. The time elapsed between the instant the activation solution was added to the powder and the paste loaded into the calorimeter was around 1 min. The tests were run for 48 h with the calorimeter set at a constant temperature of 25°C. The compressive strengths of the selected binders were determined on alkali-activated MT-S or MT-C mortar cubes in accordance with ASTM C 109. 50 mm cubes were moist cured in a chamber at 23± °C and >98% RH, and tested at the selected four different ages (3, 7, 14, and 28 days). At least three specimens from each mixture were tested for strength.

3. Models and data transformation methods

3.1. Random forest model

Random Forest (RF) model is chosen as the baseline ML model to predict hydration kinetics and compressive strength of MT-based binders, based on authors' past experience with such predictions [54–57]. Please refer to Appendix A for more details on RF models. To achieve optimal performance with the RF model, a 10-fold cross-validation (CV) method [58], [59] and grid-search method [60], [61] are employed to ascertain the optimal hyperparameters (i.e., number of trees and number of splits at each node). The 10-fold CV method involves splitting the dataset into ten subsets, training the model on nine subsets and testing it on the remaining one, repeated ten times

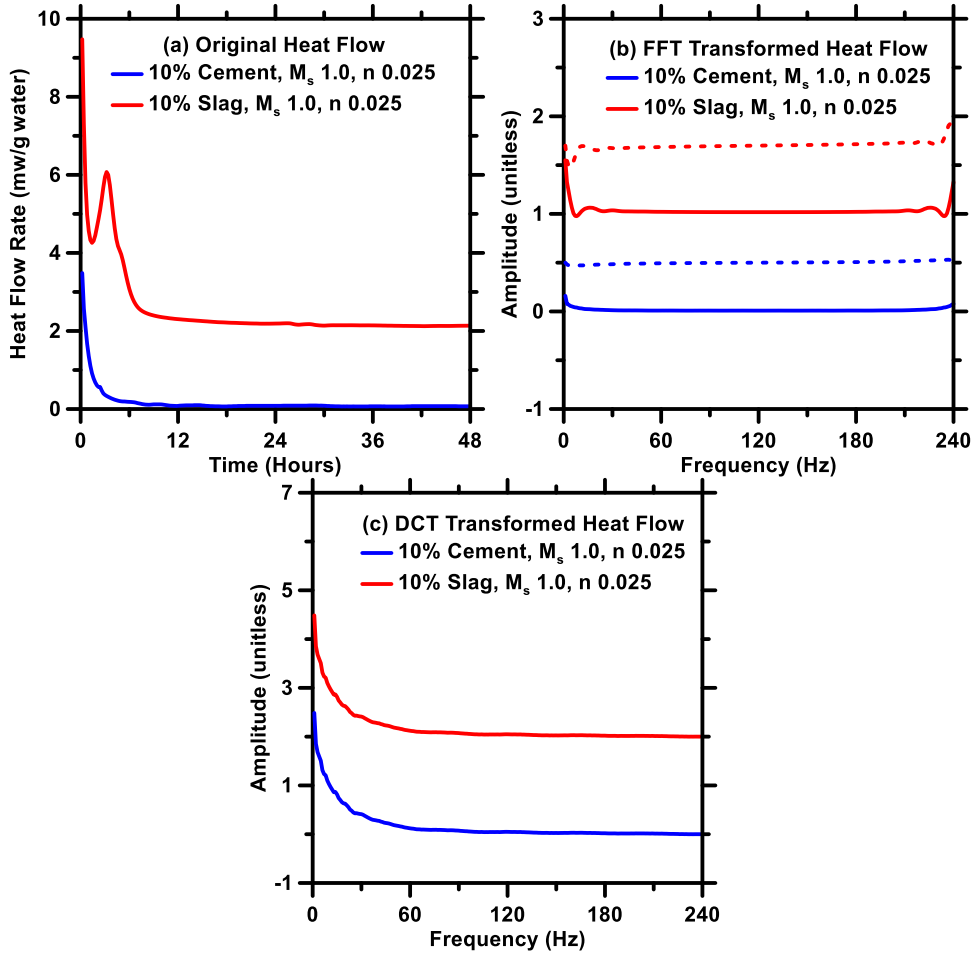

Fig. 2. (a) Original; (b) FFT-transformed (solid and dashed lines show real and imaginary components of the amplitudes, respectively); and (c) DCT-transformed heat flow rate profiles of two different MT-based binders.

for each unique combination. Simultaneously, the grid-search method systematically works through multiple combinations of *potentially optimal* hyperparameters, cross-validating as it goes to determine which combination produces the most accurate predictions. Our previous studies [55], [60], [62] have shown that the hydration kinetics of cementitious materials is too complex for a standalone ML model to produce reliable predictions. Therefore, a transformation technique is required to reduce the degrees of freedom of the hydration kinetic profiles so that the ML models can easily learn global input-output correlations instead of getting trapped at a local minimum. Our previous study [55] has demonstrated that data-transformation techniques can reduce the degrees of freedom and complexity (e.g., reduced number of inflection points in the time-dependent hydration profiles) of the training set, thereby improving prediction performance of the models. Appendix A provides detailed information on both the transformation techniques used in this study.

3.2. Fast fourier and discrete cosine transformations

Figs. 2(a) and 2(b) show the original heat flow rate profiles of MT-based binders obtained from isothermal calorimetry and their transformed counterparts obtained by fast Fourier Transform (FFT). The transformed profiles contain both real and imaginary components, which are demonstrated here. It is evident that the transformed profiles are much simpler structures (i.e., fewer inflection points and reduced peak intensities) as compared to their original counterparts. Furthermore, the inherent symmetry in the transformed profiles allows for the representation of the encoded information using significantly fewer—nearly 50% of—data points. Such data reduction is of great significance as it considerably minimizes the time and computational resources required to train the FFT-RF model.

Fig. 2(c) shows the Discrete Cosine Transform (DCT) profiles of selected MT-based binders. The transformed profiles in this case consist exclusively of real numbers. In addition to simplifying the structure of the profile, DCT substantially reduces the number of inflection points (that represent non-differentiable points) thereby making it much easier for the RF model to capture input-output correlations from the transformed profiles.

In this study, the RF model is trained using the FFT- and DCT-transformed profiles. Once trained, the model is used to predict the transformed profiles (i.e., amplitude vs. frequency) of new systems from the testing dataset (see Section 3.3) based on their inputs. Next, inverse data-transformation algorithms are used to convert the predicted transformed profiles to conventional ones (i.e., time vs. heat flow rate). The prediction performance of RF when combined with the two transformation techniques is compared. The compressive strengths of the MT-based binders are predicted by the standalone RF model.

3.3. Database

The heat flow profiles of 48 MT-based binders were obtained from isothermal calorimetry. The training dataset consists of 42 randomly selected binders, and the testing dataset includes the remaining; while ensuring no overlaps between the two datasets. For both datasets, the input variables are: MT content ($\%_{mass}$); slag content ($\%_{mass}$); cement content ($\%_{mass}$); l/b ratio (unitless); M_s (unitless); n (unitless); and time (h). Heat flow rate (mW/g water) from 0-to-48 h with a 0.2-h step size is the output. Statistical parameters summarizing the domain of the training and testing datasets are shown in Table 2. The compressive strengths of 48 MT-based binders were measured at 3, 7, 14, and 28 days. Statistical parameters interpreting the compressive strength datasets are shown in Table 3. The training dataset includes 75% of the randomly selected data records from the parent database, and the remaining data records are consolidated in the testing dataset. The input variables are the same as described earlier, except that the time (h) in the calorimetry dataset is replaced by age (day). The compressive strengths (MPa) of the binders are the output. The prediction performance of each method is evaluated by coefficient of determination (R^2); mean absolute percentage error (*MAPE*); Pearson correlation coefficient (R); mean absolute error (*MAE*); and root mean squared error (*RMSE*).

Table 2
Statistical parameters related to the training and testing dataset of heat flow rate with 8 attributes for both (7 inputs and 1 outputs).

Attribute	*Unit*	*Min.*	*Max.*	*Mean*	*Std. Dev.*
MT content	$\%_{mass}$	70	90	80	8.16
Slag content	$\%_{mass}$	0	30	10	11.55
Cement content	$\%_{mass}$	0	30	10	11.55
l/b ratio	unitless	0.35	0.55	0.39	0.07
M_s	unitless	1.0	1.5	1.25	0.25
n	unitless	0.025	0.1	0.05	0.03
Time	h	0.2	48	24.10	13.86
Output for training dataset. The database consists of 10080 unique data-records					
Heat Flow Rate	mW/g water	0.05	45.55	0.81	1.84
Output for testing dataset. The database consists of 1440 unique data-records					
Heat Flow Rate	mW/g water	0.15	16.96	0.65	1.26

Table 3
Statistical parameters related to the compressive strength dataset with 8 attributes (7 inputs and 1 outputs). The database consists of 148 unique data-records.

Attribute	*Unit*	*Min.*	*Max.*	*Mean*	*Std. Dev.*
MT content	$\%_{mass}$	70	90	81.08	8.31
Slag content	$\%_{mass}$	0	30	11.62	11.51
Cement content	$\%_{mass}$	0	30	7.30	10.31
l/b ratio	unitless	0.35	0.55	0.39	0.06
M_s	unitless	1	1.5	1.26	0.25
n	unitless	0.025	0.1	0.06	0.03
Age	day	3	28	13.00	9.51
Compressive strength	MPa	0.4	40.17	9.91	8.57

4. Results and discussions

4.1. Isothermal calorimetry

The heat flow curves for MT-S and MT-C binders are presented in Figs. 3 and 4, respectively, and succinct discussions are provided here. Table 4 shows the cumulative heat released (in mW/g water) at the end of 48 h for all MT-S and MT-C binders. The choice to express this as a function of unit mass of water, rather than that of the binder, was motivated by the latter's inability to account for variations in the l/b ratio. Note that the water includes water from the activation solution and the externally added water to achieve the desired l/b ratio. An increase in the slag or cement content leads to higher peak heat release rates and cumulative heat released, attributed to the enhanced formation of early hydration products through the combination of calcium ions (from slag/cement) and silicate ions (from sodium silicate) [63], [64]. As expected, the increase in heat release at early ages is more prominent for the MT-C binders; the heat release rate increasing in proportion to the cement content in the binder. However, after 48 h, the cumulative heat released is higher for MT-S binders except for the one prepared with a low activator alkalinity (n value of 0.025). This observation aligns with the compressive strengths of MT-S and MT-C binders as will be shown later. The binder prepared with an n value of 0.025 was observed not to set even after 12 h, indicating that the alkalinity is insufficient to dissolve the water-impermeable layer on the surface of slag particles [65]. A narrow peak within the first few hours of mixing that corresponds to the wetting and dissolution of Ca-bearing compounds, followed by a dormant period and succeeded by a smaller acceleration peak, generally attributed to the formation of reaction products such as C-S-H and C-A-S-H gels, is generally noted for the MT-S blends [36], [37], [64], [66]. For a higher M_s value (higher silicate content in the solution), the acceleration peak happens within the first

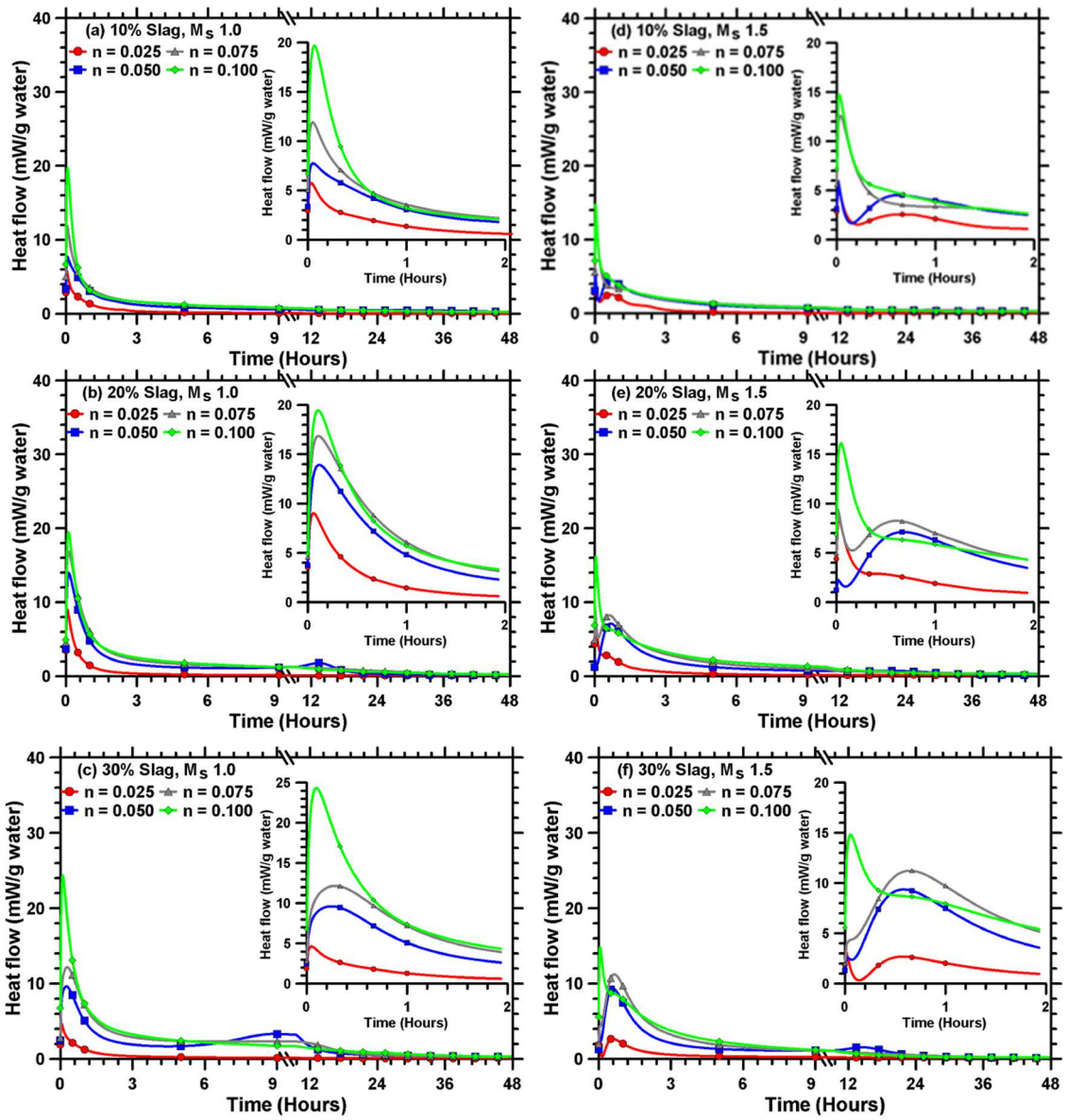

Fig. 3. Heat release rate curves for MT-S binders: M_s value of 1.0 and slag contents of: (a) 10%, (b) 20%, (c) 30%; M_s value of 1.5 and slag contents of (d) 10%, (e) 20%, (f) 30%.

hour, as shown in the figures in the inset in Fig. 3. The duration between wetting/dissolution and early product formation peaks is approximately 35 min for all the MT-S binders prepared with a M_s value of 1.5, likely due to the presence of more soluble silicates in systems with higher M_s [64]. When the alkalinity is higher (n value of 0.10), or at a lower M_s value, only a single large peak is noticed, since both these peaks merge into one. For very low alkalinity mixtures (n value of 0.025 and 0.05), a further small peak is noticed after 9–15 h, attributed to limited reaction of otherwise unreacted particles or the onset of diffusion-controlled processes.

The calorimetric response curves for MT-C binders shown in Fig. 4 exhibit patterns similar to those of the MT-S binders except for variations in the magnitudes of peak heat release rates and their temporal occurrence. Secondary peaks are observed for binders prepared with lower n values (0.025–0.05), likely corresponding to the acceleration peaks associated with cement hydration. The peak heat release rate increases for all MT-C binders as the alkalinity is increased (i.e., with higher n values at the same M_s and cement content), as more Ca^{2+} ions are introduced into the system, aiding in the formation of additional C-S-H and C-A-S-H gels. Generally, the heat release curves of the MT-C binders resemble those of dilute cement systems but exhibit early acceleration due to the influence of alkaline activators. A direct comparison among MT-C binders with different cement contents cannot be made since the l/b ratios were varied based on the cement content in the mix due to the aforementioned reasons; another reason why the heat release rates and cumulative heats are indicated in terms of unit mass of water.

4.2. Compressive strengths

The compressive strength test results for MT-S and MT-C binders are shown in Figs. 5 and 6, respectively. Binders with an initial setting time of less than 30 min or a final setting time greater than 12 h were not tested in compression. It is seen that the compressive strengths of both MT-S and MT-C binders are dependent on the activator parameters, as reported elsewhere [36], [37], and the slag or cement content in the system. The strength gain at lower alkalinity levels, i.e., n values of 0.025 and 0.05, is relatively minimal from 3 to 28 days. However, at

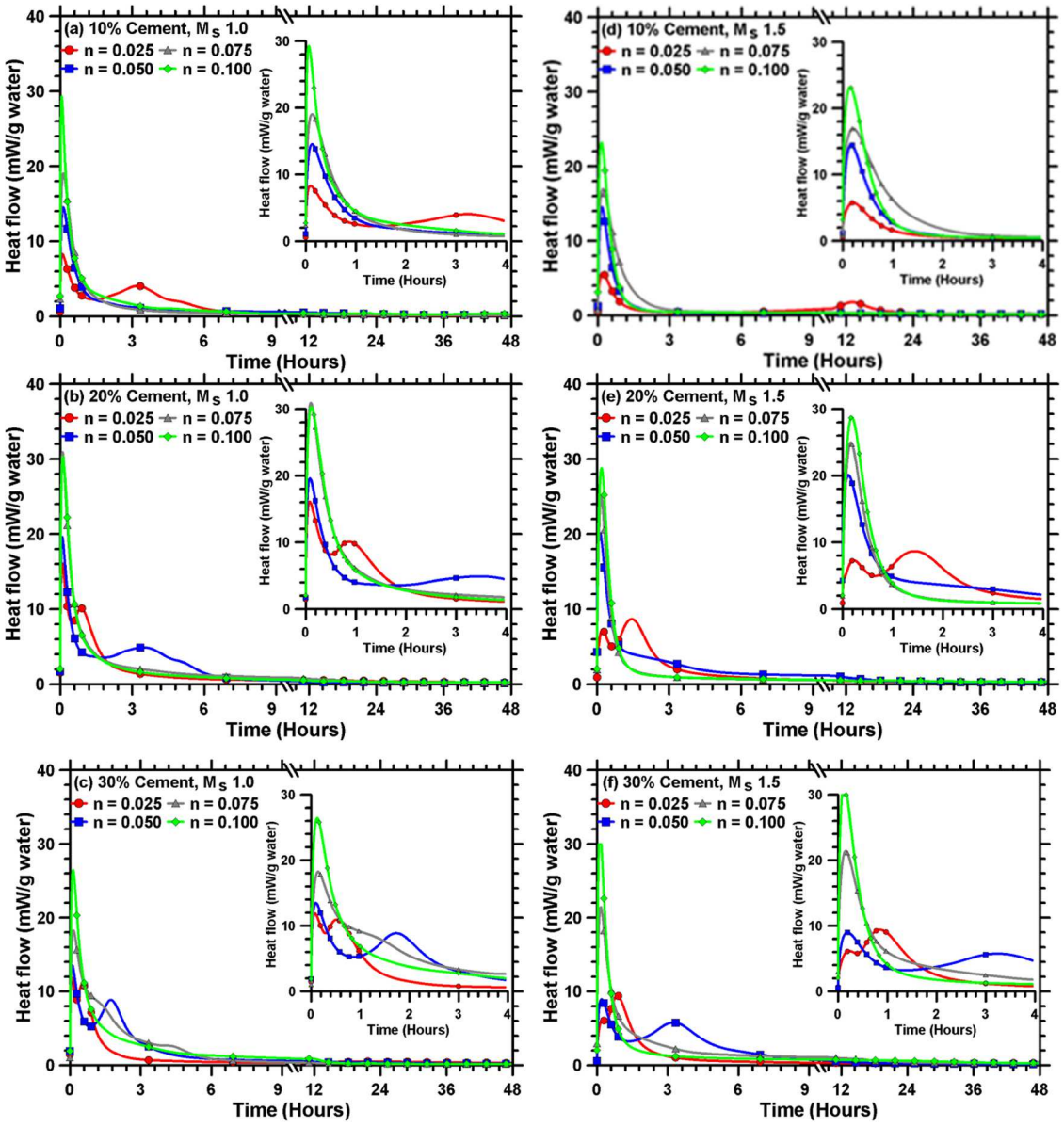

Fig. 4. Heat release rate curves for MT-C binders: M_s value of 1.0 and cement contents of: (a) 10%, (b) 20%, (c) 30%; M_s value of 1.5 and cement contents of (d) 10%, (e) 20%, (f) 30%.

Table 4
Cumulative heat released (J/g water) at the end of 48 h for MT-S and MT-C binders.

Binder system		Mass percentage of slag/cement in respective binders					
		10%		20%		30%	
	Activation parameters (n, M_s)	M_s					
		1.0	1.5	1.0	1.5	1.0	1.5
	n	Cumulative heat (J/g water)					
Mine tailings (MT) – slag (S)	0.025	29.66	36.46	39.31	48.57	36.06	48.31
	0.050	112.57	110.83	152.60	138.06	193.17	165.26
	0.075	123.40	123.89	188.26	168.49	225.17	176.14
	0.100	131.91	131.43	184.20	177.54	244.31	176.71
Mine tailings (MT) -cement (C)	0.025	97.60	101.63	139.73	138.47	120.15	106.22
	0.050	104.90	79.33	141.36	161.60	144.11	142.69
	0.075	94.33	92.43	157.44	132.96	148.35	175.98
	0.100	131.33	117.15	151.69	141.76	157.98	163.60

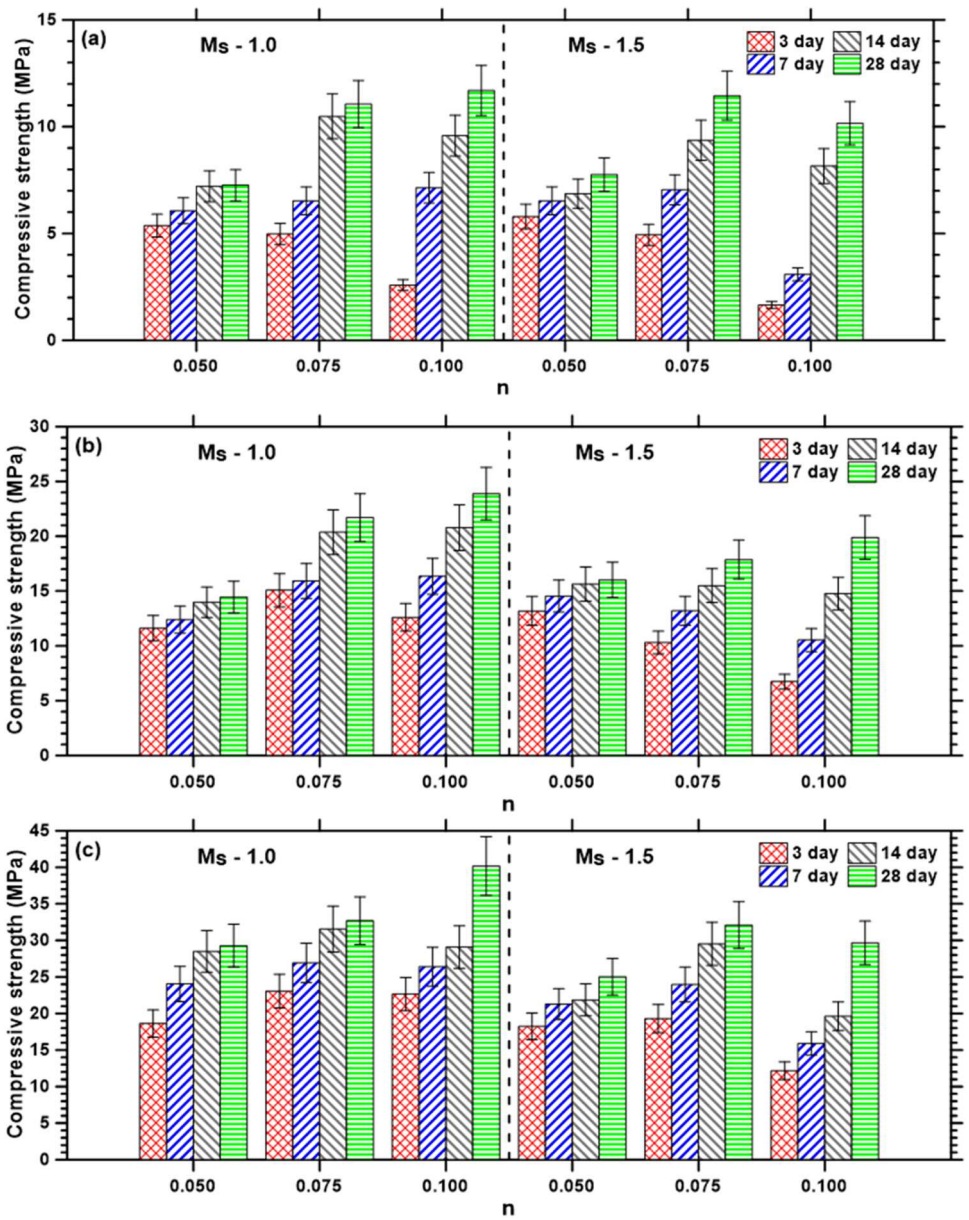

Fig. 5. Compressive strengths of MT-S binders with slag contents of: (a) 10%, (b) 20%, and (c) 30% prepared with different activator parameters (n and M_s values).

higher n values of 0.075 and 0.10, a substantial increase in strength at 14 and 28 days is observed.

Compressive strengths of MT-S binders increase significantly with increased slag contents in the mix, which is attributed to the increased formation of C-S-H and/or C-A-S-H gels. It is shown that MT-S binders comprising appropriate slag contents (~20–30%) with high volumes of MT can attain 28-day strengths of up to 40 MPa, which is sufficient for more than 90% of structural concrete applications. It is shown here that MT-S binders represents a promising approach to effectively use a large volume of MT towards achieving sustainable concretes. The 28-day compressive strengths of MT-C binders are relatively low due to the higher l/b ratios (0.40, 0.45, and 0.55) used to ensure workability and flowability.

Compressive strengths of both MT-S and MT-C binders increases with an increase in n value of the activator solution, because of the higher alkalinity that aids in the formation of more reaction products. The higher compressive strength at a higher n value can also be attributed to the formation of more silica-containing gel due to a higher concentration of sodium silicate in the activator solution, and the resultant lower Ca/Si ratio of the reaction products [51]. For MT-S binders, compressive strengths are generally found to decrease at an n and M_s combination of 0.10 and 1.5, respectively. This can be attributed to (i) the suppression of Ca^{2+} ion dissolution and/or accelerated dissolution of silica and alumina, hindering the polycondensation process (i.e., chemical condensation for producing a polymer by linking single or multiple kinds of monomers to form long chains releasing water or similar substances [67]) for hydration product formation [68], [69], and (ii) reduction in the solubility of Ca at higher alkalinity, leading to the precipitation of calcium hydroxide (CH). Similar behavior is seen for MT-C binders with 10% cement content. In such cases, where Ca^{2+} ions precipitate as CH, the strength gain is inhibited. MT-C binders with a cement content of 20% and 30% prepared with an activator solution of higher n values (0.075 and 0.1) showed a flash setting behavior due to higher NaOH concentration, as reported in another study as well, consequentially making the mix unworkable [70]. The results described here show that selecting appropriate activation parameters based on the slag or cement contents is critical to attaining desired mechanical properties.

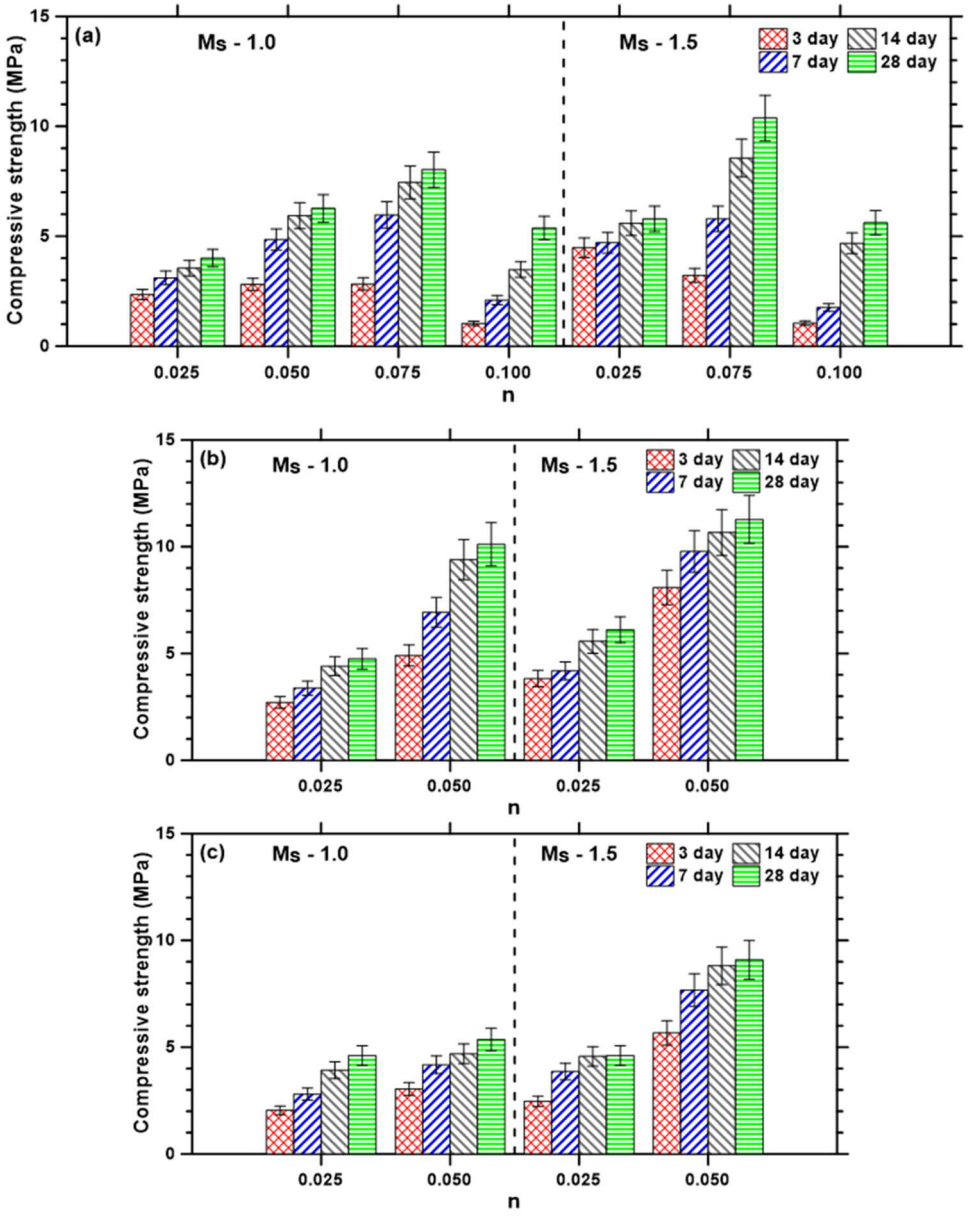

Fig. 6. Compressive strengths of MT-C binders with cement contents of: (a) 10%, (b) 20%, and (c) 30% prepared with different activator parameters (n and M_s values).

The foregoing sections demonstrate the influence of slag and cement addition on the hydration kinetics and compressive strength of MT-based binders. Previous studies [71–73] have linearly related the compressive strength and the cumulative hydration heat release of hydraulic cementitious systems, such as plain and binary OPC binders. However, such relationships for alkali-activated materials have not been reported. Fig. 7 shows the relationship between cumulative heat released at 48 h (in J/g water) and the compressive strengths of MT-S and MT-C mortars at 3, 7, 14, and 28 days; a linear relationship as reported for traditional cementitious materials is observed here as well. The cumulative heat release provides a cursory estimation of solid-to-solid connectivity within the mixture while also accounting for the inherent porosity. Since the water content is a decisive parameter influencing the porosity, the use of heat release per unit mass of the binder is further justified. Only the cumulative heat released within the initial 48 h is considered here because the hydration is most intense during this timeframe. While hydration continues beyond this period, it gradually produces solid phases (i.e., hydrates) and the heat release tends to stabilize, making further heat measurements less informative. Linear relationships between the 48 h heat release and strengths at 3, 7, 14, and 28 days serve as simple, closed-form relationships enabling reasonably-accurate predictions of compressive strength from short-duration, easy-to-conduct experiments. These relationships—albeit empirical and derived from a small number of observables—are very useful and strongly suggest that fundamental correlations that have long been used for OPC-based systems (e.g., heat vs. strength) are also applicable to highly-heterogenous binders such as MT-based alkali-activated binders. In the following section, we present direct evidence of compressive strength and hydration kinetics prediction using ML models aided by data transformation methods, based on mixture design inputs.

4.3. Heat Flow and Strength Predictions from RF Models

The FFT-RF and DCT-RF models were used to predict the heat flow rate profiles of MT-based binders, leveraging the input-output

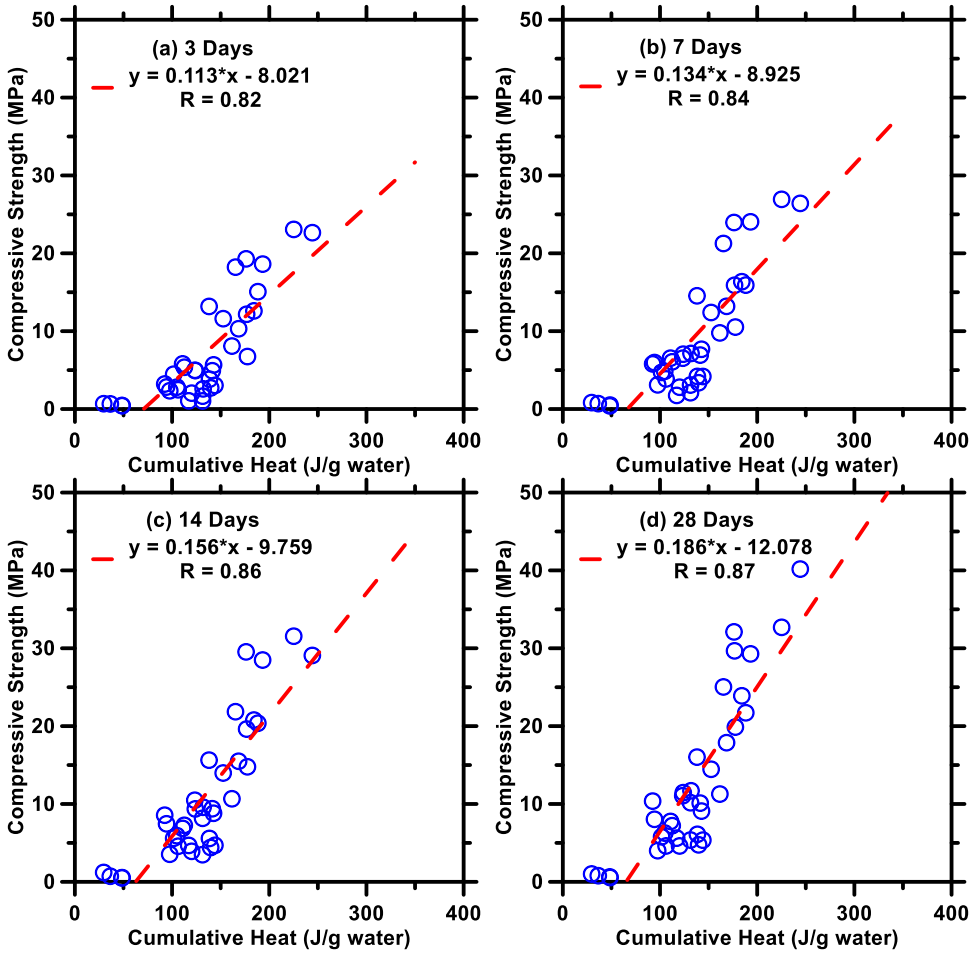

Fig. 7. Linear correlations between cumulative heat release at 48 h and compressive strengths at (a) 3 days, (b) 7 days, (c) 14 days, and (d) 28 days for MT-S and MT-C binders.

correlations learned from the training dataset. The predictions of heat flow profiles for the samples in the testing dataset obtained from FFT-RF and DCT-RF models are shown in Fig. 8. To ensure a clear and concise evaluation, logarithmic scales are employed (while the actual scale is depicted in the insets). The statistical parameters that quantify the performance of each model's prediction are shown in Table 5. It is important to emphasize that the hyperparameters within the RF component have been meticulously optimized using a combination of the 10-fold cross-validation (CV) method [58], [59] and the grid-search method [60], [61]. This approach, adopted from our previous studies, simultaneously minimizes variance (under-fitting) and bias (over-fitting), thereby enhancing the reliability of the results.

4.3.1. Heat flow rate predictions

The results presented in Table 5 and Fig. 8 demonstrate the considerable accuracy of FFT-RF and DCT-RF models in predicting the heat flow rate profiles. The findings indicate that both the DCT and FFT methods effectively reduce the degree of freedom within the database. This reduction allows the RF model to capture the intricate input-output correlations even with a relatively small dataset. However, it is worth noting that the DCT method outperforms the FFT method in terms of prediction accuracy. The superiority of the DCT method can be attributed to several reasons. The FFT method decomposes complex profiles into simpler real and imaginary number profiles, enabling the analysis of signal amplitudes and phases [74]. Consequently, the ML models are required to learn and ultimately predict both real and imaginary numbers, and the cumulative errors from predictions can further diminish the accuracy of the final output. Furthermore, the FFT method is designed to retain all the original signal details, which may result in a limited reduction in the degree of freedom for heat flow profiles of MT-based binders. The DCT method is specifically designed to compress complex signals by condensing them into a low-frequency profile represented by real numbers alone [75], [76]. Though this compression is not entirely lossless and could potentially result in the loss of pertinent information (e.g., minor shoulder peak in the calorimetry profiles), the transformed profiles thus obtained are simpler in structure compared to those obtained through FFT. This simplicity enables the RF model to readily capture the general trend within the data and yield reliable predictions. Due to solely containing real numbers, DCT method eliminates the cumulative errors associated with predicting both real and imaginary numbers. In comparison to our previous studies [54], [55], which employed techniques that reduced the complexity of the database to predict hydration kinetics of cementitious materials, the models utilized in this study shows slightly lower performance based on the *R* value. However, it is important to note that the previous studies were based on a much larger database consisting of hundreds of unique mixture designs, whereas the current study had a smaller database of only 48 mixture designs. Despite the limited database size, where ML models typically show poor performance, the predictions reported in this study show reasonable accuracy. Another point of importance is that the heat flow rates of MT-S binders are predicted more reliably by the models than the MT-C binders. This could be attributed to the fact that the cement hydration profile, especially at early ages, is more complex than that of slag activation. To further enhance the prediction performance, it is necessary to supplement a larger and more diverse training dataset.

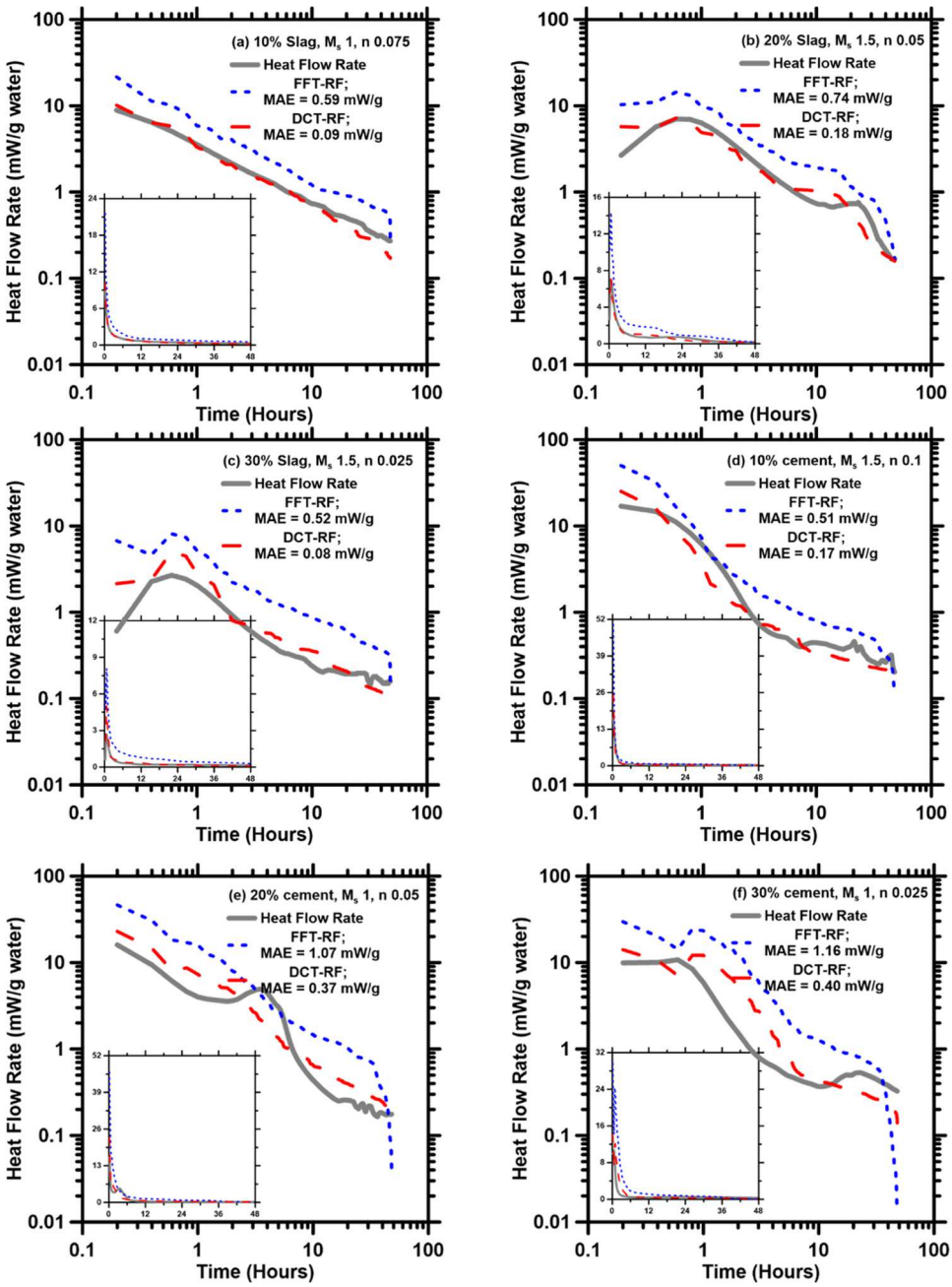

Fig. 8. Heat flow rate profile predictions of six MT-based binders as produced by FFT-RF and DCT-RF models compared against experimental measurements. The figures are plotted in logarithmic scale (with those in the insets plotted in linear scale). Mean absolute errors (*MAE*) of predictions are shown in legends.

Table 5
Five statistical parameters (average for all data records in the testing dataset) evaluating the prediction performance of FFT-RF and DCT-RF on the hydration kinetics of MT binders.

ML Model	R (Unitless)	R^2 (Unitless)	MAE (mW/g water)	MAPE (%)	RMSE (mW/g water)
FFT-RF	0.9075	0.8235	0.7682	125.1	2.175
DCT-RF	0.9184	0.8436	0.2167	30.63	0.6375

After investigating prediction performance, permutation importance method [77] is applied to reveal the influence of input variables on hydration kinetics. Based on our analyses, the top two important input variables are cement content and time. These outcomes are in agreement with hydration profiles shown in Figs. 3 and 4. Time can significantly affect the kinetics of hydration, and thus the magnitude of heat flow rate. Likewise, cement content is an important variable, considering that cement is more reactive at early ages compared to slag. Therefore, additional cement content can substantially increase the heat release.

4.3.2. *Strength predictions*

Based on the aforementioned findings, it is clear that the RF model, when combined with robust data reduction techniques, yields reliable predictions for heat flow rate profiles of MT-based binders. Encouraged by these results, the RF model is employed to predict the compressive strength of MT-based binders. The compressive strength database is split into two subsets: a training set (comprising 75% of the original database) and a testing set (comprising the remaining 25% of the original database) as mentioned earlier. Fig. 9 illustrates the predictions of the RF model for the compressive strength of MT-based binders against the

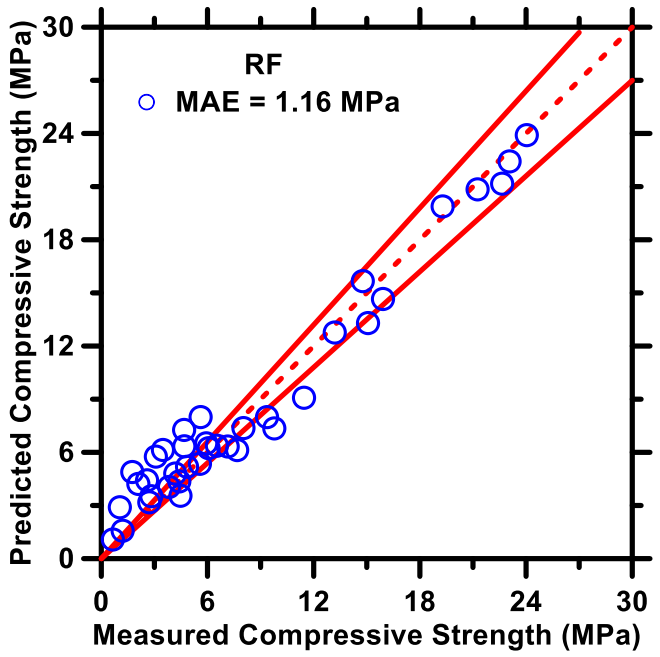

Fig. 9. The predictions performance of the RF model on the compressive strength of MT-based binders against measurements in the testing dataset. Mean absolute error (*MAE*) is shown in the legend. The solid lines are ±10% error bounds. The dashed line is the ideal predictions.

Table 6
Five statistical parameters evaluating prediction performance of RF and RF hydration on the compressive strength of MT-based binders.

ML Model	R (Unitless)	R^2 (Unitless)	MAE (MPa)	MAPE (%)	RMSE (MPa)
RF	0.9791	0.9586	1.161	31.72	1.461

measurements obtained from the testing dataset. Table 6 presents the five statistical parameters used to evaluate the prediction performance.

From the results shown in Fig. 9 and Table 6, it can be concluded that the RF model can produce reliable predictions of compressive strength of MT-based binders. The R^2 and *RMSE* values indicate a close match between the predicted and measured values, with an R^2 value of 0.96 and an *RMSE* of 1.46 MPa. It is worth noting that the general error in compressive strength measurements is reported to be around 5 MPa [78], and the prediction error is lower than the experimental error. The accurate compressive strength prediction can be attributed to the RF model's unique structure, particularly the ensemble and growth methods of decision-trees. With hundreds of uncorrelated trees in the forest, each tree generates a distinct output unaffected by other trees, effectively minimizing variance errors. Moreover, the two-stage randomization approach [79], [80] and the unpruned and unsmoothing protocols enable trees to grow with customized structures, further eliminating biases in the predictions.

Using the permutation importance method, it was found that slag and MT content exert the most influence on the compressive strength. The reactivity of MT is low, and hence its contribution to strength development also is low. Previous studies [81], [82] have shown that the compressive strength of cementitious materials monotonically decreases when the inert filler content increases. While it has been shown that MT is not just an inert filler under alkaline activation conditions [32], it is obviously not as efficient as aluminosilicates such as slag. This is also seen in Fig. 5; here, as the slag content increases from 10% to 30%, the compressive strength increases three or four fold, while a corresponding increase in cement content does not substantially alter the strength.

5. Conclusions

This study focuses on description of early-age hydration kinetics and compressive strength development of alkali-activated mine tailings (MT)-based binders. MT was used as the primary source material ($\geq$70%$_{mass}$ of total binder) in conjunction with slag (S) or cement (C) to develop MT-S or MT-C binders, respectively. The effects of varying Na_2O-to-total powder ratio (n), SiO_2-to-Na_2O ratios (M_s), and slag or cement contents on the rates of reaction and strength development were explored in detail. Isothermal calorimetry test results showed significant dependence on the activator parameters (n and M_s values) and the additive type (slag or cement) and content. Although the peak heat release is higher for MT-C binders compared to their respective MT-S counterparts at the same activator parameters and MT content, the cumulative heat released at the end of 48 h was generally higher for MT-S binders. In general, a single prominent heat release peak, corresponding to the combination of slag or cement particle wetting, dissolution, and early reaction product formation, was observed for MT-S binders prepared with a highly alkaline activator solution. In other cases, the first narrow peak within the first few hours of mixing was followed by a dormant period and succeeded by a smaller acceleration peak attributed to the formation of reaction products such as C-S-H and C-A-S-H gels. MT-S binders attained significantly higher compressive strengths than the MT-C binders. Compressive strengths of about 24 MPa and 40 MPa were attained for MT-S binders with 20% and 30% slag contents, respectively, with n and M_s values of 0.10 and 1.0, while the highest compressive strength achieved among the castable MT-C binders was approximately 11 MPa, for a mixture with 20% cement content. The cumulative heat released (per unit mass of water) at the end of 48 h was reasonably correlated with compressive strengths at different ages. This work demonstrated that carefully optimizing activator parameters and using slag as to supplement MT allows the development of MT-based binders suitable for various applications.

A random forest (RF) model was used as a ML technique to predict the heat flow rate and compressive strengths of the studied binders. Due to the complexity of hydration kinetics of binders, data-transformation techniques, namely fast Fourier transform (FFT) and discrete cosine transform (DCT), were applied to the raw heat evolution profiles to reduce the degrees of freedom of the hydration profiles. This reduction allowed the RF model to capture the input-output correlations and produce high-fidelity predictions, even with a small database. The DCT method was found to be superior to the FFT method in terms of prediction performance. The standalone RF model was used to predict the compressive strength of MT-based binders at 3, 7, 14, and 28 days. The outcomes of this work indicated that ML models coupled with data transformation techniques are a promising tool for *a priori* predictions of hydration kinetics and compressive strength of MT-based binders even when a smaller dataset is only available.

Declaration of Competing Interest

The authors declare that they have no known competing financial interests or personal relationships that could have appeared to influence the work reported in this paper.

Data Availability

Data will be made available on request.

Acknowledgements

The authors sincerely acknowledge Freeport McMoRan Inc. for supplying the mine tailings and for financial support of this work through the NSF Engineering Research Center on Bio-Mediated and Bio-Inspired Geotechnics (CBBG) at ASU (EEC 1449501). The NSF Future Manufacturing grant (DMR 2228782) is also acknowledged. The cement

and slag used in this work were supplied by Salt River Materials Group (Phoenix Cement) and Cemex, respectively, and PQ Corp supplied the sodium silicate.

Appendix A

Random Forests

The RF model is an advanced ML model with an evolution of the Classification and Regression Trees (CARTs) structure, fortified by the inclusion of the bagging technique [79], [83]—a method that subsamples the parent dataset without sacrificing the dataset volume. As part of the training process, the RF model simultaneously constructs hundreds of standalone CARTs based on bootstraps. Each tree in the forest grows by implementing binary splits in a recursive fashion, continually dividing until the terminal nodes reach a *near-homogenous* state. This process is performed without any pruning or smoothing, thereby allowing all trees to grow to their maximum size unrestrictedly. When the RF model is tasked with producing predictions on the new data domain, it averages predictions from all trees to produce the final output. The two-stage randomization [79], [80] is distinguished the RF from the traditional CARTs. The first stage of randomization pertains to the bootstrapping technique, where each tree is constructed from a randomly selected subset of the parent dataset. The second stage of randomization involves randomly choosing a subset of variables for each split. The two-stage randomization method is key in ensuring the trees within the forest are decorrelated from one another [84], [85]. This decorrelation leads to a significant reduction in variance and bias errors, enhancing the model's robustness and predictive accuracy.

Fourier Transform

The Fast Fourier Transform (FFT) is a computationally efficient method of implementing the Discrete Fourier Transform (DFT), a mathematical technique used to convert a complex signal profile from its time domain into a representation in the frequency domain, and vice versa [86], [87], [88]. This algorithm simplifies the calculation of the DFT from a complexity of N^2 to $N\,log_2N$, making it significantly faster for large data sets. The FFT takes an input in the form of a profile existing in the time domain. The algorithm then meticulously disassembles this profile into its individual sinusoidal components. Each component resonates at a unique frequency, allowing the FFT to decode the complexity of the original signal. Meanwhile, these components embody sine and cosine waves, reflecting the symmetrical nature of the frequency domain representation. Intriguingly, these separated sine and cosine waves retain the capacity to be recovered back into the original profile. The output of FFT consists of an array of complex numbers. Each number in this array embodies a specific frequency component of the original signal. These complex numbers encode two pieces of crucial information: *amplitude* and *phase*. The amplitude indicates the intensity of a frequency component, while the phase indicates the shift in time for that frequency component. More details about the FFT can be found in our previous study [55].

Discrete Cosine Transform

The Discrete Cosine Transform (DCT), developed by Ahmed et al. [89], is a mathematical function to process signal and image data by packing by compacting high-frequency coefficients to low-frequency coefficients. The DCT begins by representing data in a temporal domain, which is then transformed into the frequency domain by utilizing a series of cosine waves (which differ in frequency). The sum of those cosine waves approximates the original data. Here, the *frequency* corresponds to how fast the cosine wave oscillates, and the *amplitude* corresponds to the strength or height of the wave. In the transformed data, amplitude represents the coefficients in the cosine wave. Each coefficient captures the contribution of its corresponding cosine wave to the original signal. A high value of a coefficient means that its corresponding cosine wave contributes significantly to the original signal [90], [91]. There are several DCT functions. In this study, DCT-2 function (shown in Eq. 1) is employed to convert heat evolution profiles into low-frequency domain. δ_{k1} is the Kronecker delta; $x(n)$ is the original signal; and k represents the order of each DCT coefficient.

$$y(k) = \sqrt{\frac{2}{N}} \sum_{n=1}^{N} x(n) \frac{1}{\sqrt{1+\delta_{k1}}} \cos\left(\frac{\pi}{2N}(2N-1)(k-1)\right) \tag{1}$$

References

[1] S. Maruthupandian, A. Chaliasou, A. Kanellopoulos, Recycling mine tailings as precursors for cementitious binders – Methods, challenges and future outlook, Constr. Build. Mater. 312 (2021) 125333, https://doi.org/10.1016/j.conbuildmat.2021.125333.

[2] D. Kossoff, W.E. Dubbin, M. Alfredsson, S.J. Edwards, M.G. Macklin, K.A. Hudson-Edwards, Mine tailings dams: Characteristics, failure, environmental impacts, and remediation, Appl. Geochem. 51 (2014) 229–245, https://doi.org/10.1016/j.apgeochem.2014.09.010.

[3] C. Ince, S. Derogar, K. Gurkaya, R.J. Ball, Properties, durability and cost efficiency of cement and hydrated lime mortars reusing copper mine tailings of Lefke-Xeros in Cyprus, Constr. Build. Mater. 268 (2021) 121070, https://doi.org/10.1016/j.conbuildmat.2020.121070.

[4] A.P. Vilela, et al., Technological properties of soil-cement bricks produced with iron ore mining waste, Constr. Build. Mater. 262 (2020) 120883, https://doi.org/10.1016/j.conbuildmat.2020.120883.

[5] L. Dong, X. Tong, X. Li, J. Zhou, S. Wang, B. Liu, Some developments and new insights of environmental problems and deep mining strategy for cleaner production in mines, J. Clean. Prod. 210 (2019) 1562–1578, https://doi.org/10.1016/j.jclepro.2018.10.291.

[6] M.- Nurcholis, D.F. Yudiantoro, D.- Haryanto, A.- Mirzam, Heavy Metals Distribution in the Artisanal Gold Mining Area in Wonogiri, Art. no. 2, Indones. J. Geogr. 49 (2) (2017), https://doi.org/10.22146/ijg.15321.

[7] W. Zhou, et al., Revegetation approach and plant identity unequally affect structure, ecological network and function of soil microbial community in a highly acidified mine tailings pond, Sci. Total Environ. 744 (2020) 140793, https://doi.org/10.1016/j.scitotenv.2020.140793.

[8] A. Vasile, et al., An integrated value chain to iron-containing mine tailings capitalization by a combined process of magnetic separation, microwave digestion and microemulsion – assisted extraction, Process Saf. Environ. Prot. 154 (2021) 118–130, https://doi.org/10.1016/j.psep.2021.08.012.

[9] M.G. Macklin, et al., The long term fate and environmental significance of contaminant metals released by the January and March 2000 mining tailings dam failures in Maramureş County, upper Tisa Basin, Romania, Appl. Geochem. 18 (2) (2003) 241–257, https://doi.org/10.1016/S0883-2927(02)00123-3.

[10] M.G. Macklin, et al., A geomorphological approach to the management of rivers contaminated by metal mining, Geomorphology 79 (3) (2006) 423–447, https://doi.org/10.1016/j.geomorph.2006.06.024.

[11] M. Rico, G. Benito, A. Díez-Herrero, Floods from tailings dam failures, J. Hazard. Mater. 154 (1) (2008) 79–87, https://doi.org/10.1016/j.jhazmat.2007.09.110.

[12] H. Liu, A. Probst, B. Liao, Metal contamination of soils and crops affected by the Chenzhou lead/zinc mine spill (Hunan, China), Sci. Total Environ. 339 (1) (2005) 153–166, https://doi.org/10.1016/j.scitotenv.2004.07.030.
[13] H.M. Queiroz, et al., Manganese: The overlooked contaminant in the world largest mine tailings dam collapse, Environ. Int. 146 (2021) 106284, https://doi.org/10.1016/j.envint.2020.106284.
[14] J. Csavina, et al., A review on the importance of metals and metalloids in atmospheric dust and aerosol from mining operations, Sci. Total Environ. 433 (2012) 58–73, https://doi.org/10.1016/j.scitotenv.2012.06.013.
[15] L.S. Passos, K.G. Gnocchi, T.M. Pereira, G.C. Coppo, D.S. Cabral, L.C. Gomes, Is the Doce River elutriate or its water toxic to Astyanax lacustris (Teleostei: Characidae) three years after the Samarco mining dam collapse? Sci. Total Environ. 736 (2020) 139644 https://doi.org/10.1016/j.scitotenv.2020.139644.
[16] A.M. Salam, B. Örmeci, P.H. Simms, Determination of optimum polymer dosage for dewatering of oil sands tailings using torque rheology, J. Pet. Sci. Eng. 197 (2021) 107986, https://doi.org/10.1016/j.petrol.2020.107986.
[17] G. Lazorenko, A. Kasprzhitskii, F. Shaikh, R.S. Krishna, J. Mishra, Utilization potential of mine tailings in geopolymers: Physicochemical and environmental aspects, Process Saf. Environ. Prot. 147 (2021) 559–577, https://doi.org/10.1016/j.psep.2020.12.028.
[18] X. He, et al., Mine tailings-based geopolymers: A comprehensive review, Ceram. Int. 48 (17) (2022) 24192–24212, https://doi.org/10.1016/j.ceramint.2022.05.345.
[19] S. Zhao, M. Xia, L. Yu, X. Huang, B. Jiao, D. Li, Optimization for the preparation of composite geopolymer using response surface methodology and its application in lead-zinc tailings solidification, Constr. Build. Mater. 266 (2021) 120969, https://doi.org/10.1016/j.conbuildmat.2020.120969.
[20] N. Zhang, A. Hedayat, H.G. Bolaños Sosa, J.J. González Cárdenas, G.E. Salas Álvarez, V.B. Ascuña Rivera, Specimen size effects on the mechanical behaviors and failure patterns of the mine tailings-based geopolymer under uniaxial compression, Constr. Build. Mater. 281 (2021) 122525, https://doi.org/10.1016/j.conbuildmat.2021.122525.
[21] A. Barzegar Ghazi, A. Jamshidi-Zanjani, H. Nejati, Utilization of copper mine tailings as a partial substitute for cement in concrete construction, Constr. Build. Mater. 317 (2022) 125921, https://doi.org/10.1016/j.conbuildmat.2021.125921.
[22] A.M.T. Bagger, W. Kunther, N.M. Sigvardsen, P.E. Jensen, Screening for key material parameters affecting early-age and mechanical properties of blended cementitious binders with mine tailings, Case Stud. Constr. Mater. 15 (2021) e00608, https://doi.org/10.1016/j.cscm.2021.e00608.
[23] R.S. Krishna, F. Shaikh, J. Mishra, G. Lazorenko, A. Kasprzhitskii, Mine tailings-based geopolymers: Properties, applications and industrial prospects, Ceram. Int. 47 (13) (2021) 17826–17843, https://doi.org/10.1016/j.ceramint.2021.03.180.
[24] Z. Xiaolong, Z. Shiyu, L. Hui, Z. Yingliang, Disposal of mine tailings via geopolymerization, J. Clean. Prod. 284 (2021) 124756, https://doi.org/10.1016/j.jclepro.2020.124756.
[25] A. Saedi, A. Jamshidi-Zanjani, A.K. Darban, M. Mohseni, H. Nejati, Utilization of lead–zinc mine tailings as cement substitutes in concrete construction: Effect of sulfide content, J. Build. Eng. 57 (2022) 104865, https://doi.org/10.1016/j.jobe.2022.104865.
[26] Y. Zhu, Z. Wang, Z. Li, H. Yu, Experimental research on the utilization of gold mine tailings in magnesium potassium phosphate cement, J. Build. Eng. 45 (2022) 103313, https://doi.org/10.1016/j.jobe.2021.103313.
[27] L. Reig, L. Soriano, M.M. Tashima, M.V. Borrachero, J. Monzó, J. Payá, Influence of calcium additions on the compressive strength and microstructure of alkali-activated ceramic sanitary-ware, J. Am. Ceram. Soc. 101 (7) (2018) 3094–3104, https://doi.org/10.1111/jace.15436.
[28] J. Temuujin, A. van Riessen, R. Williams, Influence of calcium compounds on the mechanical properties of fly ash geopolymer pastes, J. Hazard. Mater. 167 (1) (2009) 82–88, https://doi.org/10.1016/j.jhazmat.2008.12.121.
[29] S.A. Bernal, J.L. Provis, Durability of Alkali-Activated Materials: Progress and Perspectives, J. Am. Ceram. Soc. 97 (4) (2014) 997–1008, https://doi.org/10.1111/jace.12831.
[30] F. Pacheco-Torgal, J. Castro-Gomes, S. Jalali, Alkali-activated binders: A review: Part 1. Historical background, terminology, reaction mechanisms and hydration products,", Constr. Build. Mater. 22 (7) (2008) 1305–1314, https://doi.org/10.1016/j.conbuildmat.2007.10.015.
[31] P. Duxson, A. Fernández-Jiménez, J.L. Provis, G.C. Lukey, A. Palomo, J.S.J. van Deventer, Geopolymer technology: the current state of the art, J. Mater. Sci. 42 (9) (2007) 2917–2933, https://doi.org/10.1007/s10853-006-0637-z.
[32] X. Tian, F. Rao, C.A. León-Patiño, S. Song, Co-disposal of MSWI fly ash and spent caustic through alkaline-activation: Immobilization of heavy metals and organics, Cem. Concr. Compos. 114 (2020) 103824, https://doi.org/10.1016/j.cemconcomp.2020.103824.
[33] F. Zhang, Y. Li, J. Zhang, X. Gui, X. Zhu, C. Zhao, Effects of slag-based cementitious material on the mechanical behavior and heavy metal immobilization of mine tailings based cemented paste backfill, Heliyon 8 (9) (2022) e10695, https://doi.org/10.1016/j.heliyon.2022.e10695.
[34] J.G.S. Van Jaarsveld, J.S.J. Van Deventer, L. Lorenzen, The potential use of geopolymeric materials to immobilise toxic metals: Part I. Theory and applications, Miner. Eng. 10 (7) (1997) 659–669, https://doi.org/10.1016/S0892-6875(97)00046-0.
[35] Z. Zhang, J.L. Provis, J. Zou, A. Reid, H. Wang, Toward an indexing approach to evaluate fly ashes for geopolymer manufacture, Cem. Concr. Res. 85 (2016) 163–173, https://doi.org/10.1016/j.cemconres.2016.04.007.
[36] D. Ravikumar, N. Neithalath, Reaction kinetics in sodium silicate powder and liquid activated slag binders evaluated using isothermal calorimetry, Thermochim. Acta 546 (2012) 32–43, https://doi.org/10.1016/j.tca.2012.07.010.
[37] S. Chithiraputhiran, N. Neithalath, Isothermal reaction kinetics and temperature dependence of alkali activation of slag, fly ash and their blends, Constr. Build. Mater. 45 (2013) 233–242, https://doi.org/10.1016/j.conbuildmat.2013.03.061.
[38] Z. Zhang, J.L. Provis, A. Reid, H. Wang, Fly ash-based geopolymers: The relationship between composition, pore structure and efflorescence, Cem. Concr. Res. 64 (2014) 30–41, https://doi.org/10.1016/j.cemconres.2014.06.004.
[39] W.K.W. Lee, J.S.J. van Deventer, Structural reorganisation of class F fly ash in alkaline silicate solutions,", Colloids Surf. Physicochem. Eng. Asp. 211 (1) (2002) 49–66, https://doi.org/10.1016/S0927-7757(02)00237-6.
[40] T. Bakharev, Durability of geopolymer materials in sodium and magnesium sulfate solutions, Cem. Concr. Res. 35 (6) (2005) 1233–1246, https://doi.org/10.1016/j.cemconres.2004.09.002.
[41] T. Bakharev, Geopolymeric materials prepared using Class F fly ash and elevated temperature curing, Cem. Concr. Res. 35 (6) (2005) 1224–1232, https://doi.org/10.1016/j.cemconres.2004.06.031.
[42] B. Singh, G. Ishwarya, M. Gupta, S.K. Bhattacharyya, Geopolymer concrete: A review of some recent developments, Constr. Build. Mater. 85 (2015) 78–90, https://doi.org/10.1016/j.conbuildmat.2015.03.036.
[43] K.T. Nguyen, Q.D. Nguyen, T.A. Le, J. Shin, K. Lee, Analyzing the compressive strength of green fly ash based geopolymer concrete using experiment and machine learning approaches, Constr. Build. Mater. 247 (2020) 118581, https://doi.org/10.1016/j.conbuildmat.2020.118581.
[44] M. Lahoti, P. Narang, K.H. Tan, E.-H. Yang, Mix design factors and strength prediction of metakaolin-based geopolymer, Ceram. Int. 43 (14) (2017) 11433–11441, https://doi.org/10.1016/j.ceramint.2017.06.006.
[45] D.V. Dao, H.-B. Ly, S.H. Trinh, T.-T. Le, B.T. Pham, Artificial Intelligence Approaches for Prediction of Compressive Strength of Geopolymer Concrete, Art. no. 6, Materials 12 (6) (2019), https://doi.org/10.3390/ma12060983.
[46] P.R. Prem, A. Thirumalaiselvi, M. Verma, "Applied linear and nonlinear statistical models for evaluating strength of Geopolymer concrete,", Comput. Concr. 24 (1) (2019) 7–17, https://doi.org/10.12989/cac.2019.24.1.007.
[47] S. Yin, Z. Yan, X. Chen, R. Yan, D. Chen, J. Chen, Mechanical properties of cemented tailings and waste-rock backfill (CTWB) materials: Laboratory tests and deep learning modeling, Constr. Build. Mater. 369 (2023) 130610, https://doi.org/10.1016/j.conbuildmat.2023.130610.
[48] B. Zhang, K. Li, S. Zhang, Y. Hu, B. Han, Strength prediction and application of cemented paste backfill based on machine learning and strength correction, Heliyon 8 (8) (2022) e10338, https://doi.org/10.1016/j.heliyon.2022.e10338.
[49] C.B. Arachchilage, C. Fan, J. Zhao, G. Huang, W.V. Liu, A machine learning model to predict unconfined compressive strength of alkali-activated slag-based cemented paste backfill, J. Rock. Mech. Geotech. Eng. (2023), https://doi.org/10.1016/j.jrmge.2022.12.009.
[50] A. Dakhane, S. Das, S. Kailas, N. Neithalath, Elucidating the Crack Resistance of Alkali-Activated Slag Mortars Using Coupled Fracture Tests and Image Correlation, J. Am. Ceram. Soc. 99 (1) (2016) 273–280, https://doi.org/10.1111/jace.13960.
[51] K. Vance, M. Aguayo, A. Dakhane, D. Ravikumar, J. Jain, N. Neithalath, Microstructural, Mechanical, and Durability Related Similarities in Concretes Based on OPC and Alkali-Activated Slag Binders, Art. no. 4, Int. J. Concr. Struct. Mater. 8 (4) (2014), https://doi.org/10.1007/s40069-014-0082-3.
[52] S. Surehali, A. Simon, R.K. Ramasamy, N. Neithalath, A Comparison of the Effect of Activator Cations (Sodium and Potassium) on the Fresh and Hardened Properties of Mine Tailing-Slag Binders, Art. no. 4, Constr. Mater. 3 (4) (2023), https://doi.org/10.3390/constrmater3040025.
[53] L. Li, J. Xie, B. Zhang, Y. Feng, J. Yang, A state-of-the-art review on the setting behaviours of ground granulated blast furnace slag- and metakaolin-based alkali-activated materials, Constr. Build. Mater. 368 (2023) 130389, https://doi.org/10.1016/j.conbuildmat.2023.130389.
[54] T. Han, et al., Deep learning to predict the hydration and performance of fly ash-containing cementitious binders, Cem. Concr. Res. 165 (2023) 107093, https://doi.org/10.1016/j.cemconres.2023.107093.
[55] T. Han, S.A. Ponduru, R. Cook, J. Huang, G. Sant, A. Kumar, A Deep Learning Approach to Design and Discover Sustainable Cementitious Binders: Strategies to Learn From Small Databases and Develop Closed-form Analytical Models, Front. Mater. 8 (2022) 796476, https://doi.org/10.3389/fmats.2021.796476.
[56] S.A. Ponduru, T. Han, J. Huang, A. Kumar, Predicting Compressive Strength and Hydration Products of Calcium Aluminate Cement Using Data-Driven Approach, Art. no. 2, Materials 16 (2) (2023), https://doi.org/10.3390/ma16020654.
[57] R. Bhat, et al., Predicting compressive strength of alkali-activated systems based on the network topology and phase assemblages using tree-structure computing algorithms, Constr. Build. Mater. 336 (2022) 127557, https://doi.org/10.1016/j.conbuildmat.2022.127557.
[58] R. Cook, J. Lapeyre, H. Ma, A. Kumar, Prediction of Compressive Strength of Concrete: A Critical Comparison of Performance of a Hybrid Machine Learning Model with Standalone Models,", ASCE J. Mater. Civ. Eng. 31 (11) (2019) 04019255 https://doi.org/10.1061/(ASCE)MT.1943-5533.0002902.
[59] C. Schaffer, Selecting a classification method by cross-validation, Mach. Learn. 13 (1) (1993) 135–143, https://doi.org/10.1007/BF00993106.
[60] J. Lapeyre, et al., Machine Learning Enables Prompt Prediction of Hydration Kinetics of Multicomponent Cementitious Systems, Sci. Rep. 11 (3) (2021) 3922, https://doi.org/10.1038/s41598-021-83582-6.
[61] E. Gomaa, T. Han, M. ElGawady, J. Huang, A. Kumar, Machine Learning to Predict Properties of Fresh and Hardened Alkali-activated Concrete, Cem. Concr. Compos. 115 (1) (2021) 103863, https://doi.org/10.1016/j.cemconcomp.2020.103863.

[62] R. Cook, et al., Machine learning for high-fidelity prediction of cement hydration kinetics in blended systems, Mater. Des. 208 (2021) 109920, https://doi.org/10.1016/j.matdes.2021.109920.
[63] D. Jiang, C. Shi, Z. Zhang, Recent progress in understanding setting and hardening of alkali-activated slag (AAS) materials, Cem. Concr. Compos. 134 (2022) 104795, https://doi.org/10.1016/j.cemconcomp.2022.104795.
[64] C. Shi, R.L. Day, A calorimetric study of early hydration of alkali-slag cements, Cem. Concr. Res. 25 (6) (1995) 1333–1346, https://doi.org/10.1016/0008-8846(95)00126-W.
[65] R. Obenaus-Emler, M. Falah, M. Illikainen, Assessment of mine tailings as precursors for alkali-activated materials for on-site applications, Constr. Build. Mater. 246 (2020) 118470, https://doi.org/10.1016/j.conbuildmat.2020.118470.
[66] Y. Zuo, G. Ye, Preliminary Interpretation of the Induction Period in Hydration of Sodium Hydroxide/Silicate Activated Slag,", Mater. Basel Switz. 13 (21) (2020) 4796, https://doi.org/10.3390/ma13214796.
[67] A. Autef, E. Joussein, G. Gasgnier, S. Rossignol, Role of the silica source on the geopolymerization rate: A thermal analysis study, " *J. Non-Cryst. Solids* 366 (2013) 13–21, https://doi.org/10.1016/j.jnoncrysol.2013.01.034.
[68] G.F. Huseien, M. Ismail, N.H.A. Khalid, M.W. Hussin, J. Mirza, Compressive strength and microstructure of assorted wastes incorporated geopolymer mortars: Effect of solution molarity, Alex. Eng. J. 57 (4) (2018) 3375–3386, https://doi.org/10.1016/j.aej.2018.07.011.
[69] T. Phoo-ngernkham, V. Sata, S. Hanjitsuwan, C. Ridtirud, S. Hatanaka, P. Chindaprasirt, High calcium fly ash geopolymer mortar containing Portland cement for use as repair material, Constr. Build. Mater. 98 (2015) 482–488, https://doi.org/10.1016/j.conbuildmat.2015.08.139.
[70] L. Manjarrez, A. Nikvar-Hassani, R. Shadnia, L. Zhang, Experimental Study of Geopolymer Binder Synthesized with Copper Mine Tailings and Low-Calcium Copper Slag, J. Mater. Civ. Eng. 31 (8) (2019) 04019156, https://doi.org/10.1061/(ASCE)MT.1943-5533.0002808.
[71] Z. Li, D. Lu, X. Gao, Analysis of correlation between hydration heat release and compressive strength for blended cement pastes, Constr. Build. Mater. 260 (2020) 120436, https://doi.org/10.1016/j.conbuildmat.2020.120436.
[72] A. Kuryłowicz-Cudowska, Correlation between Compressive Strength and Heat of Hydration of Cement Mortars with Siliceous Fly Ash, Art. no. 11, Minerals 12 (11) (2022), https://doi.org/10.3390/min12111471.
[73] H. Thiyagarajan, A. Karunanithi, Investigation on the Correlation Between Heat Release and Compressive Strength Development in Fly Ash–Cement Composites, J. Inst. Eng. India Ser. A 101 (1) (2020) 77–87, https://doi.org/10.1007/s40030-019-00404-9.
[74] K.R. Rao, D.N. Kim, J.-J. Hwang, *Fast Fourier Transform - Algorithms and Applications*. in Signals and Communication Technology, Springer Netherlands,, Dordrecht, 2010, https://doi.org/10.1007/978-1-4020-6629-0.
[75] N. Roma, L. Sousa, A tutorial overview on the properties of the discrete cosine transform for encoded image and video processing, Signal Process 91 (11) (2011) 2443–2464, https://doi.org/10.1016/j.sigpro.2011.04.015.
[76] W.A. Mustafa, et al., Image Enhancement Based on Discrete Cosine Transforms (DCT) and Discrete Wavelet Transform (DWT): A Review, IOP Conf. Ser. Mater. Sci. Eng. 557 (1) (2019) 012027, https://doi.org/10.1088/1757-899X/557/1/012027.
[77] C. Strobl, A.-L. Boulesteix, T. Kneib, T. Augustin, A. Zeileis, "Conditional variable importance for random forests,", BMC Bioinforma. 9 (1) (2008) 307, https://doi.org/10.1186/1471-2105-9-307.
[78] E. Nawy, Ed., *Concrete Construction Engineering Handbook*. CRC Press, 2008. doi: 10.1201/9781420007657.
[79] L. Breiman, , "Random forests,", Mach. Learn. 45 (1) (2001) 5–32, https://doi.org/10.1023/A:1010933404324.
[80] A. Liaw, M. Wiener, Classif. Regres. Random 23 (2001).
[81] C.S. Poon, C.S. Lam, The effect of aggregate-to-cement ratio and types of aggregates on the properties of pre-cast concrete blocks, Cem. Concr. Compos. 30 (4) (2008) 283–289, https://doi.org/10.1016/j.cemconcomp.2007.10.005.
[82] L. Gündüz, The effects of pumice aggregate/cement ratios on the low-strength concrete properties, Constr. Build. Mater. 22 (5) (2008) 721–728, https://doi.org/10.1016/j.conbuildmat.2007.01.030.
[83] L. Breiman, Bagging predictors, Mach. Learn. 24 (2) (1996) 123–140, https://doi.org/10.1007/BF00058655.
[84] L. Gãš. Biau, Devroye, G.ãą. Lugosi, "Consistency of random forests and other averaging classifiers,", J. Mach. Learn. Res 9 (2008) 2015–2033.
[85] X. Chen, H. Ishwaran, Random forests for genomic data analysis, Genomics 99 (6) (2012) 323–329, https://doi.org/10.1016/j.ygeno.2012.04.003.
[86] R.J. Higgins, Fast Fourier transform: An introduction with some minicomputer experiments, Am. J. Phys. 44 (8) (1976) 766–773, https://doi.org/10.1119/1.10128.
[87] G.D. Bergland, "A guided tour of the fast Fourier transform,", IEEE Spectr. 6 (7) (1969) 41–52, https://doi.org/10.1109/MSPEC.1969.5213896.
[88] W.T. Cochran *et al.*, "What is the fast Fourier transform?," *Proc. IEEE*, vol. 55, no. 10, pp. 1664–1674, Oct. 1967, doi: 10.1109/PROC.1967.5957.
[89] N. Ahmed, T. Natarajan, K.R. Rao, "Discrete Cosine Transform,", IEEE Trans. Comput. C–23 (1) (1974) 90–93, https://doi.org/10.1109/T-C.1974.223784.
[90] G. Strang, The Discrete Cosine Transform, SIAM Rev. 41 (1) (1999) 135–147, https://doi.org/10.1137/S0036144598336745.
[91] K.R. Rao, P.C. Yip, Discrete cosine transform: algorithms, advantages, applications, Academic Press,, Boston, 1990.